Nano Energy 95 (2022) 106996

Contents lists available at ScienceDirect

Nano Energy

journal homepage: www.elsevier.com/locate/nanoen

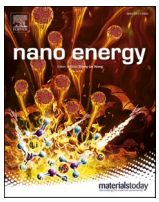

A large-area versatile textile for radiative warming and biomechanical energy harvesting

Yi Zhang [1,a], Yang Li [1,b], Keqiao Li [b], Ye Seul Kwon [b], Thilhara Tennakoon [a], Cunteng Wang [a], Ka Chung Chan [a,*], Sau-Chung Fu [a], Baoling Huang [b,*], Christopher Y.H. Chao [c]

[a] Department of Mechanical Engineering, The University of Hong Kong, Pokfulam, Hong Kong, China
[b] Department of Mechanical and Aerospace Engineering, The Hong Kong University of Science and Technology, Clear Water Bay, Kowloon, Hong Kong, China
[c] Department of Mechanical Engineering and Department of Building Environment and Energy Engineering, The Hong Kong Polytechnic University, Hong Kong, China

ARTICLE INFO

Keywords:
Personal thermal management
Triboelectric nanogenerators
Textiles
Thermal radiation
Energy harvesting

ABSTRACT

Both thermal management and electricity generation are becoming two basic functions for next-generation clothing integrated with wearable electronics. However, such versatile textiles with a simple design and great comfort have been rarely reported. Here, we propose a tri-layer textile that not only realizes solar and passive radiative warming but also harvests biomechanical energy to generate electricity. The textile is achieved by assembling photothermal nanoparticles on an infrared-reflective and conductive fabric with a tribo-negative polytetrafluoroethylene (PTFE) nanofiber membrane on the backside. The textile offers both a minimal thermal emissivity (down to 11.0%) and a maximum solar absorptivity (up to 83.7%), effectively suppressing radiation heat loss and boosting the harvested solar-thermal energy. Wearing such a textile enables a 3 °C drop of the indoor heating setpoint compared to a cotton textile, saving 25.2–100% of building energy consumption in ten cities worldwide. Moreover, the textile can serve as a single-electrode triboelectric nanogenerator. Remarkably high outputs (150–352 V, 7.5–27.8 μA) can be attained upon hand touching with different forces (14.7–44.0 N) and frequencies (0.9–3.9 Hz), which can power 41 LEDs. This textile opens a promising direction on how to develop a multifunctional energy-saving and electricity-generation textile while keeping thermal comfort for wearers.

1. Introduction

Clothing, a necessity of our daily life, has three basic functions including protection, modesty, as well as warmth. In terms of the warming function, conventional clothing can only reduce heat dissipation from the human body to the cold environment through convection and conduction. In frigid outdoor environments, heavy clothes have to be worn to maintain the body temperature and avoid discomfort and even hypothermia, which are inconvenient especially for those outdoor workers and sports enthusiasts. For indoor environments, to keep the body warm, space heating powered by non-renewable energy is generally used, wherein the majority of the energy is wasted on heating the space instead of the human body. According to the report of Ürge-Vorsatz et al., buildings contributed to 41% of the total energy consumption in the US, out of which 16–28% was used for heating [1,2]. Therefore, functional textiles that can locally achieve thermal regulation of the human body not only play a vital role in human comfort and health but also contribute significantly to reducing energy consumption. Moreover, with the popularity of wearable electronics, powering these emerging wearable electronics is becoming another basic function of next-generation clothing. However, so far, there are few reports on such versatile textiles that can simultaneously achieve the two basic functions, i.e., highly efficient body warming and electricity generation.

Over the past several years, functional textiles that are capable of managing the radiation heat transfer have aroused great attention [3–10]. In fact, thermal radiation, instead of conduction and convection, dominates the whole heat transfer between human bodies and the environment in most cases. It is reported that 40–60% of the heat generated by human bodies is dissipated via IR radiation, but conventional textiles such as cotton and polyesters cannot suppress radiative heat losses due to their high surface emissivity ($\varepsilon_{textile} \sim 0.90$) [4,11–14]. For passive radiative warming, suppression of the human body radiation

* Corresponding authors.
E-mail addresses: mekcchan@hku.hk (K.C. Chan), mebhuang@ust.hk (B. Huang).
[1] Yi Zhang and Yang Li contributed equally to this work.

https://doi.org/10.1016/j.nanoen.2022.106996
Received 11 December 2021; Received in revised form 15 January 2022; Accepted 27 January 2022
Available online 31 January 2022

to the environment is the key [11]. Therefore, recently, low-emissivity textiles were designed to block radiative heat dissipation of human body and realize passive radiative warming effects [3–9]. Moreover, when people are outdoors with solar radiation, the textile should make use of solar energy by converting solar radiation into heat for body warming. For example, in Fig. 1a, the temperatures in January of ten major cities worldwide were listed. These cities have monthly average ambient temperatures of about −3–16 ℃, which are well below the comfort temperature. We can also note that the solar radiation intensities at noon of these cities are about 600–900 W m^{-2}. For a typical day in January in Beijing (Fig. 1b), the temperature is from −7 to 4 ℃, while the highest solar radiation is up to 800 W m^{-2}. Therefore, in general, an ideal textile that can keep the body warm in most scenarios should satisfy two criteria: 1) the heat of the textile and skin would not be radiated to the environment; 2) the textile can efficiently absorb sunlight and convert it into heat.

On the other hand, wearable electronics integrated with clothing have achieved considerable advances in recent decades to meet the requirements of motion tracking [15–18], health monitoring [19–23], and so on. Batteries can be used to power these wearable devices; however, most of the batteries are large, heavy, non-flexible, and non-washable. In addition, batteries need to be charged frequently. Self-powered systems that harvest energy from the ambient environment have been demonstrated to address these issues [24–31]. Since mechanical movement is always involved in human activities, harvesting the ubiquitous and constantly available biomechanical energy is another attractive strategy for providing a continuous power. For this purpose, textile triboelectric nanogenerators (textile-TENGs) have been developed to harvest the biomechanical motion of bodies [32–39]. However, the thermal comfort of wearing textile-TENGs has never been taken into considerations, which is a matter of health and life.

It is highly preferable if the two basic functions (radiative body warming and electricity generation) can be integrated into commercially available textiles without compromising their wearability and comfort. To this end, in this study, we proposed a tri-layer (~140 μm in thickness) low-emissivity TENG (LET) textile that can passively keep the body warm in both indoor and outdoor environments (solar absorption ~ 83.7%, thermal emissivity ~16.0%) and generate electricity from body motions. The LET-textile contains a layer of photothermal titanium nitride (TiN) nanoparticles (NPs) thin film, a conductive Cu/Ni coated polyester fabric, and an electrospinning polytetrafluoroethylene (PTFE) nanofiber membrane. This textile has several advantages over other textile technologies as shown in Fig. 1c: (1) excellent warming ability under both indoor and outdoor (under sunlight irradiation) environments enabled by both passive and solar radiative warming; (2) feasible for large-scale fabrication and low cost due to facile fabrication methods; (3) electricity generation from biomechanical energy through triboelectric nanogenerators. This work proposed an effective and simple approach to develop a versatile textile that can provide thermal comfort and generate electricity from body motions at the same time.

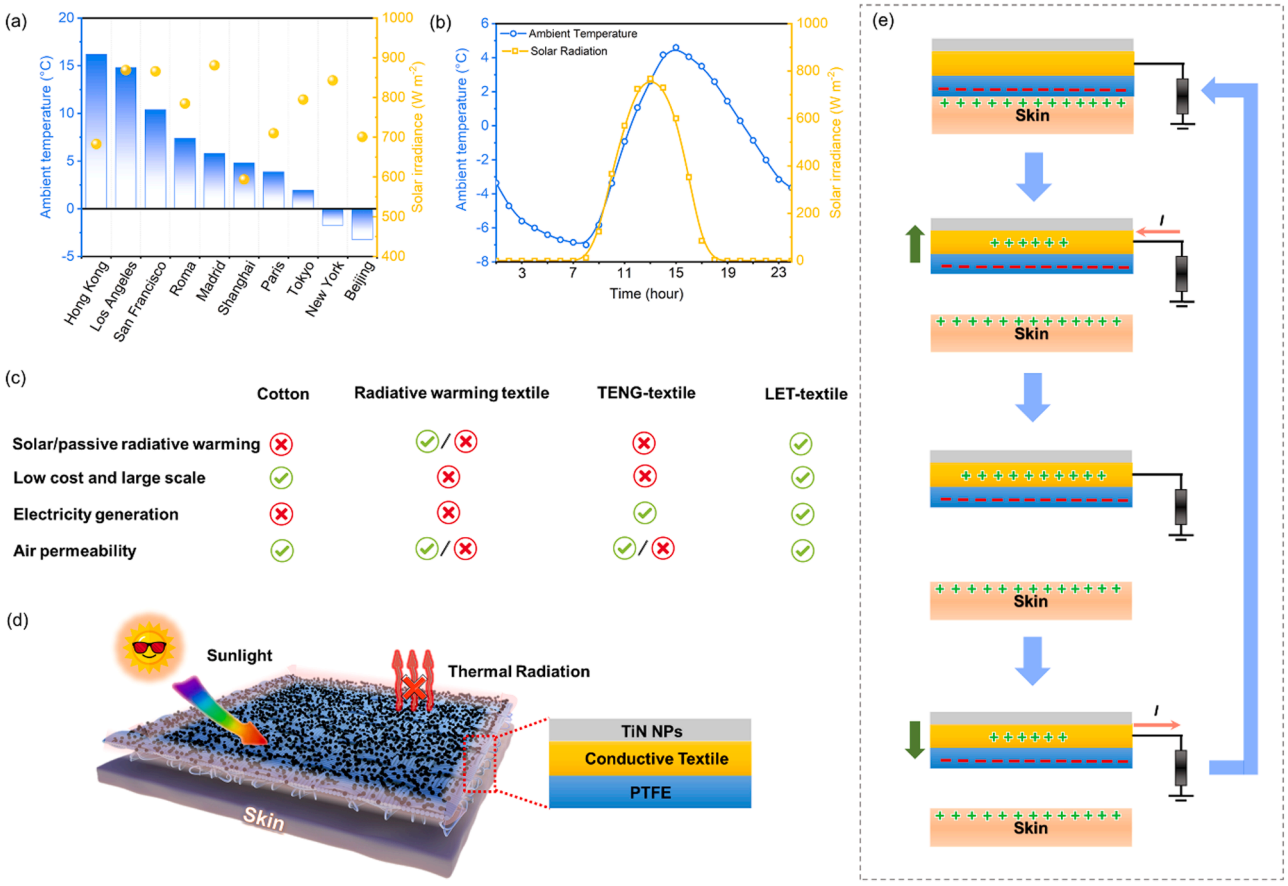

Fig. 1. The concept of LET-textile. (a) The average ambient temperatures and average daytime solar irradiances in January of 10 major cities worldwide. (b) The trend of ambient temperature and solar irradiance for one day in January in Beijing. (c) The comparison of four different textile techniques regarding 4 criteria. (d) Schematic diagram of the proposed LET-textile to keep the body warm by both a passive approach (low thermal emissivity) and an active approach (high solar absorptivity). The LET-textile has three layers: a photothermal TiN layer, an IR-reflective fabric, and a PTFE nanofiber layer. (e) Schematic diagram of the LET-textile to generate electricity by human motions.

2. Results and discussion

2.1. Working mechanism of the LET-textile

The solar irradiance spectrum is mainly distributed in the UV, visible, and near-infrared (IR) range spanning from 0.3 to 4 μm. Human skin is a natural IR emitter with an ultrahigh emissivity of 98%. At the skin temperature of 33 ℃, the human body emits thermal radiation in the mid-IR region with a peak wavelength of 9.5 μm. The LET-textile is expected to offer a high UV, visible and near-IR absorptivity but a low mid-IR emissivity, indicating great spectral selectivity, which is challenging especially on porous substrates. To achieve the functions of both radiative warming and energy harvesting from body motions, we proposed a tri-layer LET-textile that consists of a solar-absorbing film of TiN NPs, an IR-reflective and electrically conductive Cu/Ni coated polyester textile, and a PTFE nanofiber membrane. The PTFE layer is only for energy generation purpose since PTFE is almost the most tribo-negative material in the triboelectric series [40]. The Cu/Ni coated conductive textile (CT) is the key to achieving two functions together in such a simple structure. On one hand, it has a low electrical resistance (R_s = 0.037 Ωsq^{-1}) and can serve as an electrode for TENG. On the other hand, its high reflectivity of 97% in the mid-IR region (> 2.5 μm) is ideal in serving as a substrate to attain a low emissivity textile. TiN nanoparticles have strong capability in absorbing broad-spectrum solar photons enabled by localized surface plasmon resonance and locally converting them into heat. Colloidal TiN nanoparticles were spray-coated on the CT to form a uniform solar-absorbing thin film [41]. As illustrated in Fig. 1d, outdoor with solar radiation, the LET-textile keeps the body warm by absorbing the sunlight, as well as minimizing the radiative heat loss because of its low mid-IR emissivity. Moreover, in indoor places or outdoor places without solar radiation, the LET-textile can passively maintain the body temperature by suppressing the heat loss via thermal radiation to the cold environment. In short, clothes made of the LET-textile can be worn against the cold in various scenarios because of the dual-ability in solar and passive warming. In addition, the breathability of the textile is guaranteed as all three layers are porous or made of fibers. The air permeability of LET-textile is 17 $cm^3\ s^{-1}\ cm^{-2}$ at pressure drop of 100 Pa (Fig. S1b in supporting information), which is better than some other textile-TENGs [42–46]. In addition, the water vapor can also penetrate through LET-textile, and the transmission rate is 12 mg $cm^{-2}\ h^{-1}$, which is comparable to that of cotton, 13 mg $cm^{-2}\ h^{-1}$ (Fig. S1c in supporting information).

The principle of electricity generation of LET-textile is shown in Fig. 1e. The LET-textile can be actuated by skin touching and working in the TENG single-electrode mode. PTFE is the charge-induced layer for generating electricity. A commercial PTFE nanofiber membrane (Sterlitech PTFE23001, 0.2 μm) (the morphology is shown in Fig. S2, supporting information) is fabricated by electrospinning; therefore, the large surface area of the membrane can greatly enhance the surface charge density when electrification happens [47]. Specifically, the working mechanism is schematically illustrated on the combination of the contact triboelectrification and the electrostatic effect. When the skin contacts the PTFE nanofiber membrane, charges will transfer from the skin to the PTFE membrane. Once a relative separation occurs between the skin and the PTFE membrane, the negative charges on the surface of the PTFE membrane will induce positive charges on the CT to compensate the triboelectric charges, driving free electrons to flow from the CT to the ground. The role of ground could be replaced by a large size reference electrode or with the human body as the conduit [48,49]. This electrostatic induction process can generate an output voltage/current signal. When the negative triboelectric charges on the PTFE membrane are completely balanced by the induced positive charges on the CT, no output signals are produced. When the skin approaches the PTFE membrane again, the induced positive charges on the fabric electrode decrease, which causes the electrons to flow from the ground to the CT until the skin and the PTFE membrane becomes fully in contact with each other again, resulting in a reversed output signal and completing a full cycle of the electricity generation process. With periodic touches on the textile, alternating electricity outputs can be continuously generated. Since the electric potential between skin and PTFE is not large enough to cause electrostatic discharge, no discomfort will happen during the electricity generation.

2.2. Fabrication of the LET-textile

TiN is an emerging plasmonic material. Compared to those conventional plasmonic nanoparticles such as Au and Ag, TiN nanoparticles have a broader absorption band and stronger absorption intensity in the visible wavelength due to the larger imaginary part of the dielectric constant as shown in Fig. S3 in the supplementary information [50]. The plasmon resonance (the resonance wavelength, the resonance intensity, and the bandwidth) of TiN depends on the nanoparticle size. To study the effects of the TiN nanoparticle size on the optical performance of the LET-textiles, we performed the Finite-Difference Time-Domain (FDTD) simulations for the LET-textiles with TiN nanoparticles of various sizes (20, 30, 40, 60, and 80 nm). An optimal nanoparticle size of around 30 nm was selected in this work (Fig. S4).

As shown in Fig. 2a, the solar-absorbing thin film made of TiN nanoparticles was spray-coated on the plasma-treated hydrophilic CT. Then, the CT and the PTFE nanofiber membrane were attached together by hot pressing with a small amount of adhesive fabric. The use of adhesive fabrics does not affect the air permeability of the textile since it is a highly loose fusible nonwoven fabric with pores of hundreds of micrometers (Fig. S5). In addition, the air permeability of adhesive fabrics (430 $cm^3\ s^{-1}\ cm^{-2}$) is much higher than LET-textile (17 $cm^3\ s^{-1}\ cm^{-2}$). Both the uniformity and thickness of TiN nanoparticle film are of critical importance to the optical performance of the textile [41]. However, it is technically challenging by spray-coating to achieve such a nanoparticle film, because the pristine morphology of the CT textile is quite rough, and its wettability is poor. To address these problems, O_2 plasma was employed to improve the surface hydrophilicity, and the coating process was performed at an elevated temperature (60 °C) to accelerate the solvent evaporation. Then, desired TiN nanoparticle thin films can be achieved by optimizing the coating parameters, such as the coating cycles (or runs), the flow rate, the nozzle height, the nozzle speed to name just a few (Fig. S6).

By using this scalable fabrication process, a large-area textile (0.3 × 0.3 m^2) was produced (Fig. 2b). By wearing the LET-textile (Fig. S7), the human body can achieve a comfortable temperature of ~ 40 °C on a winter day (air temperature of 17 °C) with weak sunlight (300 W m^{-2}). In Fig. 2c and d, the SEM images show that TiN nanoparticles are conformally coated on the CT fabric yarn and form a uniform and smooth thin film, which is also confirmed by the EDX mapping results (Fig. S8). The TiN nanoparticles in this study were ball-milled together with the propylene glycol methyl ether acetate (PGMEA). After being coated, the nanoparticles can be bonded by the PGMEA tightly so that they cannot fall off from the textile. Moreover, the rough surface of the textile is also beneficial for anti-abrasion. As shown in Fig. 2e, at a flow rate of 0.1 ml min^{-1}, the absorptivity spectra of textiles' outer surfaces gradually change with the increase of the coating run. More importantly, all of them show spectral selectivity as expected: high absorption for shorter wavelengths and reduced absorption for longer mid-IR wavelengths, as shown in Fig. 2f. The absorption spectrum of the textile's inner surface is shown in Fig. S9, supporting information.

To quantitatively evaluate the overall optical performance of the textiles of different processes, their spectrally averaged solar absorptivity α_{solar} and thermal emissivity ε were calculated. The α_{solar} was defined as:

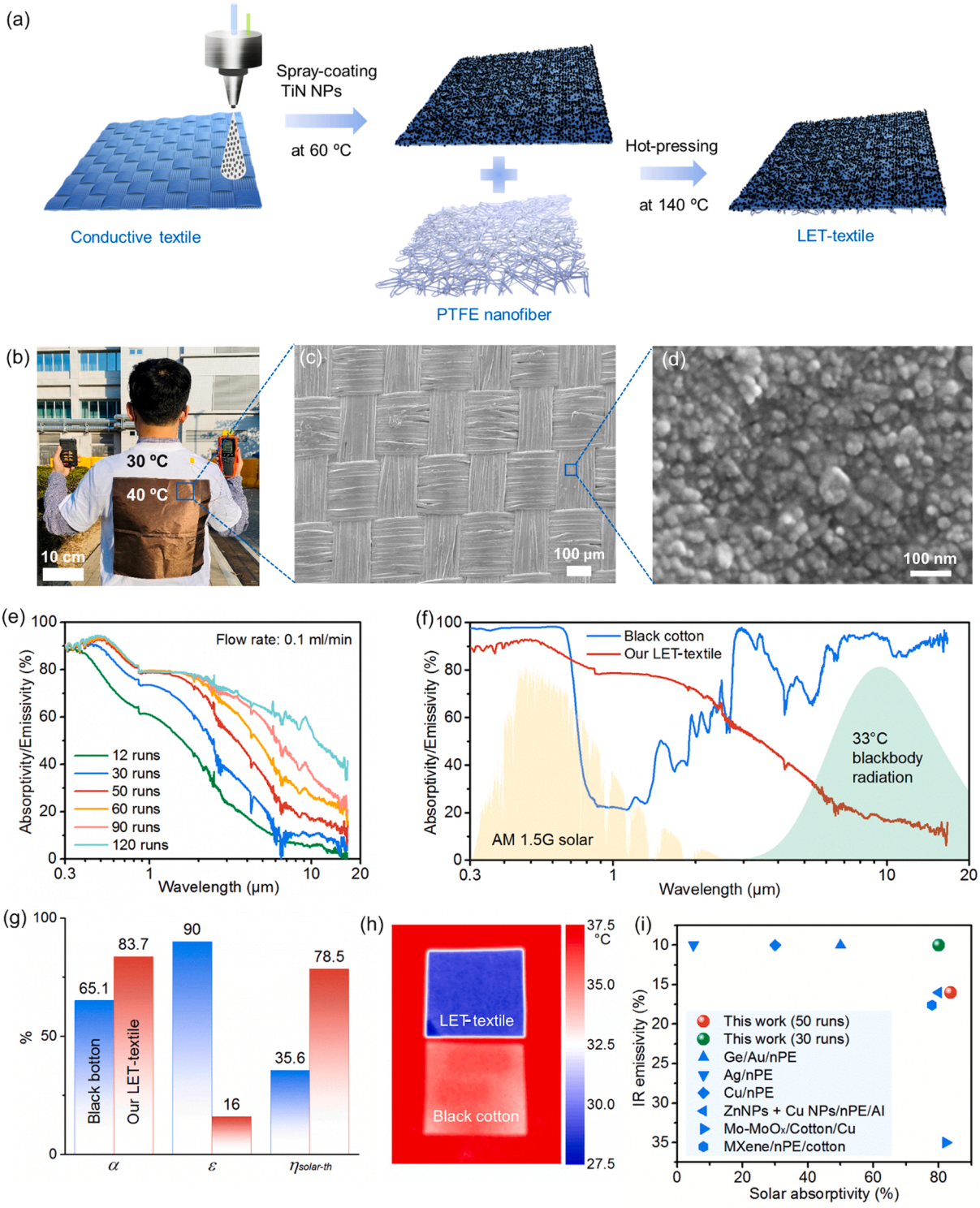

Fig. 2. Fabrication process, morphology and optical performance of LET-textile. (a) Fabrication process flow of the LET-textile. (b) Demonstration of a large-area (0.3×0.3 m^2) LET-textile on a human body in a cold environment. (c) SEM image of the LET-textile (the conductive textile side). (d) High-resolution SEM image of the TiN nanoparticles. (e) Absorptivity/emissivity spectra of LET-textiles coated with TiN nanoparticles for different coating runs. (f) Absorptivity/emissivity spectra of both the LET-textile coated with TiN nanoparticles for 50 runs and the black cotton, together with the AM 1.5G solar spectrum, as well as the radiation spectrum of a human body with a skin temperature of 33 °C. (g) Spectrally averaged solar absorptivity α, thermal emissivity ε at 33 °C, and the solar-thermal energy conversion efficiency $\eta_{solar\text{-}th}$ at a typical January day (at 11:00 am) in Beijing, when the solar irradiation intensity is 0.57 sun and the ambient temperature is −1 °C. (h) IR photographs of LET-textile and black cotton on a hot plate (37.5 °C). The ambient temperature is 25 °C. (i) Comparison of both the solar absorptivity and the IR emissivity between our LET-textiles (50 and 30 runs) and reported textiles, including Ge/Au/nPE [3], Ag/nPE [6], Cu/nPE [4], ZnNPs+CuNPs/nPE/Al [7], Mo-MoO_x/cotton/Cu [8], and MXene/nPE/cotton [9]. The solar absorptivity for Ag/nPE and Cu/nPE are calculated from Ag and Cu film, respectively. The data for MXene/nPE/cotton are calculated from its absorption spectrum.

$$\alpha_{solar} = \frac{\int_{0.3\mu m}^{4\mu m} \alpha(\lambda) AM_{1.5G}(\lambda) d\lambda}{\int_{0.3\mu m}^{4\mu m} AM_{1.5G}(\lambda) d\lambda}, \quad (1)$$

and the ε was defined as

$$\varepsilon(T) = \frac{\int_{0.3\mu m}^{20\mu m} \varepsilon(\lambda) E_b(\lambda, T) d\lambda}{\sigma T^4} \quad (2)$$

Here $AM_{1.5}(\lambda)$, $E_b(\lambda, T)$, $\alpha_{solar}(\lambda)$, and $\varepsilon(\lambda)$ represent the spectral solar power ($AM_{1.5}$), the emission power of a blackbody with a temperature T, the solar absorptivity, and the emissivity at the wavelength λ, respectively. ε is calculated at a typical skin temperature of 33 °C [5]. As shown in Fig. 2f and g, the LET-textile of 50 runs manifests both a high α_{solar} of 83.7% and a low $\varepsilon_{33\,^\circ C}$ of 16.0%. As a comparison, the black cotton shows a lower α_{solar} of 65.1% due to the narrow solar absorption band, as well as a much higher $\varepsilon_{33\,^\circ C}$ of 90% owing to its strong mid-IR absorption. The black cotton was chosen as the control sample since cotton is one of the most common textiles and black color offers the highest visible light absorptivity among different colors.

To compare the solar warming ability of the LET-textile and black cotton, we calculated their solar-to-thermal energy conversion efficiency $\eta_{solar\text{-}th}$ using the following equation [51]:

$$\eta_{solar-th}(T) = \alpha_{solar} - \varepsilon \frac{\sigma(T^4 - T_0{}^4)}{C \times I_{solar}} \quad (3)$$

where I_{solar} is the intensity of AM 1.5 G solar power, i.e., 1000 W m^{-2}, C is the solar concentration, and T_0 is the ambient temperature. Taking a typical winter day in Beijing, China as an example, as shown in Fig. 1b, the solar irradiance is around 570 W m^{-2} (i.e., $C = 0.57$) at 11:00 am and the ambient temperature is around −1.0 °C. In these conditions, the black cotton can only offer a quite low $\eta_{solar\text{-}th}$ of 35.6% due to the massive thermal radiation heat loss (169 W m^{-2}), while our LET-textile (50 runs) offers a more than two times higher $\eta_{solar\text{-}th}$ of 78.5% enabled by the significantly suppressed radiation heat loss (30 W m^{-2}). In addition, our LET-textile of 30 runs offers an even lower $\varepsilon_{33\,^\circ C}$ of 11.0% compared to that of 50 runs, as well as a α_{solar} of 81.0%, yielding a comparable $\eta_{solar\text{-}th}$ of 77.4%. Therefore, the LET-textile of 50 runs is more suitable for solar warming, while that of 30 runs is more suitable for passive warming without sunlight due to the lower $\varepsilon_{33\,^\circ C}$. To intuitively compare their thermal emissivity, the LET-textiles and black cotton were attached on a hot plate with a constant temperature of 37.5 °C, and were observed by a thermal imager with the default emissivity of 0.95, as shown in Fig. 2h. The LET-textile appears to be much cooler than the black cotton and as cool as the environment (ambient temperature is 25 °C), indicating the low emissivity of the LET-textile. The optical performance of our LET-textiles (both 50 and 30 runs) is also the best among reported state-of-the-art solar-absorbing textiles (Fig. 2i).

In addition, we measured the mechanical strength of LET-textile (Fig. S10). A 4 mm (width) by 140 μm (thickness) LET-textile strip can endure a maximum tensile force of 30 N, which means that the ultimate strength is 52 MPa as shown in Fig. S10b in the supplementary information. These results are better than the nanoPE-based smart textile [6,9]. To further demonstrate the mechanical stability of LET-textile, tearing and cyclic tensile tests were also conducted to measure fracture energy and shape recovery properties. Based on the results shown in Fig. S10c in the supplementary information, the fracture energy of LET-textile is about 42,857 J m^{-2}. In addition, the LET-textile exhibits good shape recovery from large deformation. LET-textile recovers 68.4%, 63.1%, and 65.6% from the cycles involving 5%, 10%, and 15% of tensile strain, respectively as shown in Fig. S10d in the supplementary information.

2.3. Warming performance of LET-textile

We evaluated the warming performance of the textile using a power-controllable silicone heater that simulates the heat generation of skin inside a large temperature-controllable room (8 × 4 × 3 m^3). Since the silicone heater has an emissivity similar to the real skin, it was used as the artificial skin to simulate the heat transfer of the real human skin [4]. A constant heat flux of 110 W m^{-2} was applied to the artificial skin to simulate the heat generation from the human body, and a thermocouple was attached to the skin surfaces as shown in Fig. 3a. The LET-textile and the control group (black cotton) had the same thickness during the whole experiment. The first step of the test is to determine the minimum ambient temperature (MAT) that can be set without compromising human thermal comfort. Thermal comfort means that the skin temperature maintains at 33 ℃ to keep the body core temperature at around 37 ℃ and the heat produced by the body is dissipated to the environment when covered with different textiles. Without solar radiation, the measured thermostat temperature of the room was 20.1 °C for the black cotton, and 17.8 °C for the LET-textile to maintain the skin temperature at 33 °C as shown in Fig. 3b. Due to its low emissivity, our LET-textile shows better passive warming ability than the cotton and can save energy by lowering the indoor temperature point where air-conditioners or heating installations have to be turned on.

The second step of the field test is to evaluate the performance of the textile with solar radiation by adopting a solar simulator to simulate the outdoor case. The temperature of the artificial skin was recorded when wearing black cotton and LET-textile under different solar irradiance (200–1000 W m^{-2}, monitored by a solar meter). The temperature of the control room was set from 15 to 5 °C. As shown in Fig. 3c–e, when the ambient temperature was set as 15, 10, or 5 °C, the skin temperature with our LET-textile at the steady state was always much higher than that with black cotton (with the same thickness) under different solar irradiation intensities, i.e., 0.2, 0.4, 0.6, 0.8, and 1.0 sun. For instance, when the ambient temperature is 15 °C, the skin temperature with the LET-textile is around 35 °C under weak sunlight of 0.2 kW m^{-2}. However, to realize such a comfortable skin temperature with black cotton, a relatively stronger illumination of 0.6 sun is needed at 15 °C (Fig. 3c). Moreover, as shown in Fig. 3c–e, under the illumination of 0.4 sun and the ambient temperature of 15, 10, and 5 °C, the steady-state skin temperatures with black cotton are 32.0, 27.5, and 24.0 °C, respectively. In other words, a person wearing black cotton begins to feel cold when the ambient temperature is below 15 °C, although there is a solar irradiation of 400 W m^{-2}. However, wearing the LET-textile under the same solar irradiation, a person still feels warm even when the ambient temperature is as low as 5 °C, because the skin temperature is maintained at 35 °C (Fig. 3e). Fig. 3f and g map the skin temperatures with the black cotton and our LET-textile as functions of both the solar irradiation intensity and ambient temperature. Clearly, our LET-textile can maintain the skin temperature $\geq$ 33 °C in most of the frigid conditions with weak solar irradiation and low ambient temperatures (>0.35 sun at 5 °C, and >0.30 sun at 10 °C). As a comparison, black cotton is only suitable in cases with both strong solar irradiation and high temperatures (e.g., > 0.43 sun at 15 °C, and > 0.72 sun at 10 °C).

2.4. Heat transfer model

The warming ability without and with solar radiation has been demonstrated by experiments in Section 2.3. However, the MAT under different conditions, such as heat transfer inside the air gap, convective heat transfer coefficient between textile and ambient h_e, metabolic heat generation q_{gen}, and the thickness of air gap between textile and skin t_a are still unknown. Therefore, we used one-dimensional steady-state heat transfer model analysis to determine the MAT under different scenarios. Although this model has been used in some previous studies [4,6,7,11,52], it needs to be modified for our multifunctional LET-textile. We modified the model on two aspects: 1. LET-textile has

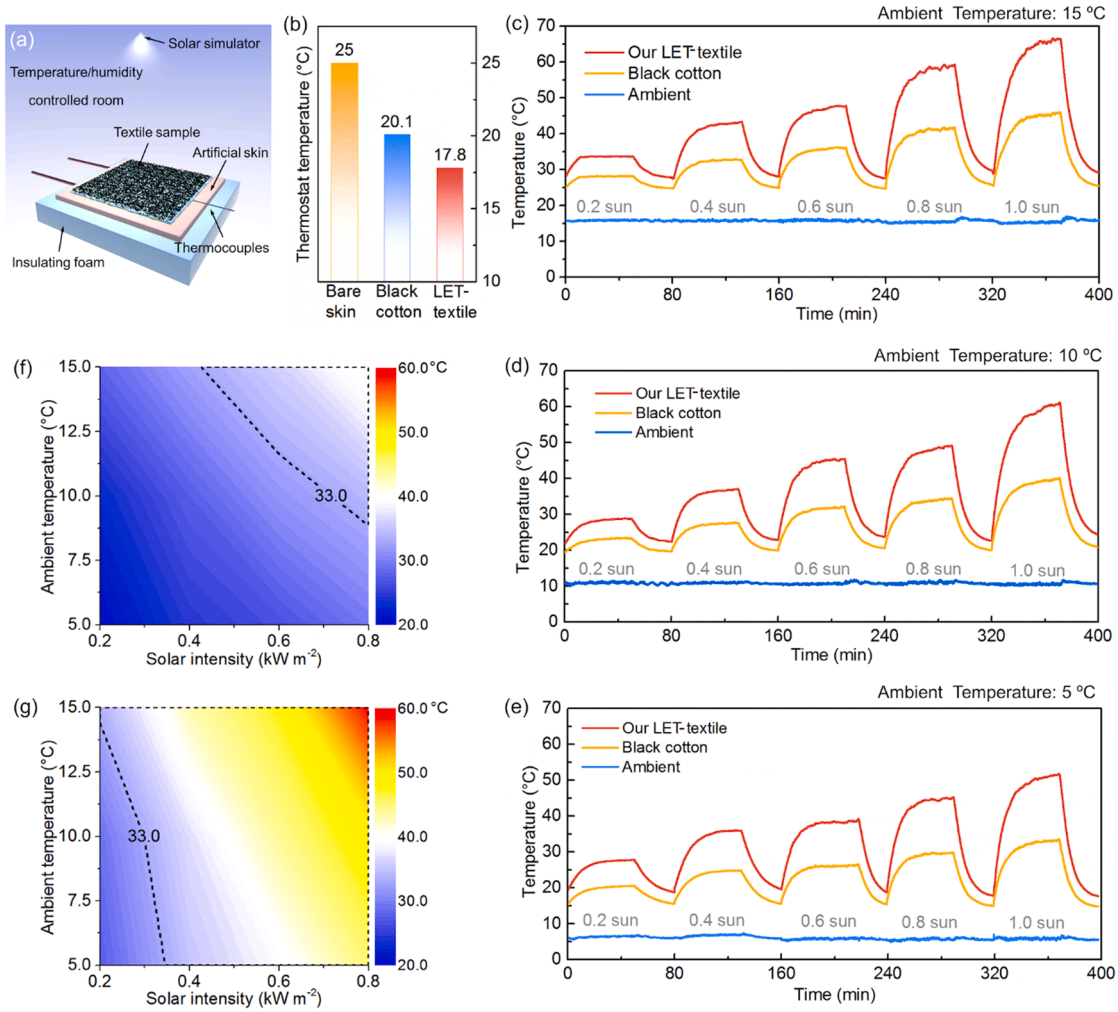

Fig. 3. Solar and passive warming performance tests in an environmentally controlled room. (a) Schematic of the experiment setup of passive warming (without solar irradiation) and active solar warming (with solar irradiation) performance tests in the temperature/humidity controlled room ($8 \times 4 \times 3$ m^3). (b) Measured thermostat temperatures of bare skin, skin with black cotton, as well as skin with the LET-textile. (c–e) Measured skin temperature of both the LET-textile covered skin and black cotton covered skin under illuminations of 0.2, 0.4, 0.6 and 0.8 sun at different ambient temperatures: (c) 15 °C, (d) 10 °C and (e) 5 °C. (f) Skin temperatures with black cotton as functions of both solar intensity and ambient temperature. (g) Skin temperatures with our LET-textile as functions of both solar intensity and ambient temperature.

zero transmittance in both solar wavelength and IR region; 2. Since the LET-textile needs to move to generate electricity, the movement will cause air to flow inside the textile/skin air gap, thus the assumption that only heat conduction occurs in the air gap will not be valid. Therefore, heat convective inside the air gap will also be considered. The model is illustrated in Fig. 4a. The parameters used in the model are listed in Table S1 in supporting information. There are three unknown parameters in the model, i.e., the temperature of ambient, textile outer surface, and textile inner surface.

Since convective heat transfer cannot be ignored inside the air gap, a Nusselt number was used to characterize the heat transfer in the air gap. Nusselt number from 1 (only conduction) to 20 was examined. Our LET-textile has a lower MAT than black cotton in the whole range of the Nusselt number. A larger Nusselt number means stronger heat transfer inside the air gap; therefore, a higher MAT is needed to sustain the skin temperature at 33 ℃. Since convection is caused by air and body movements, the h_e varies with air velocity and walking speed [53] from 10 to 20 W m^{-2} K^{-1} for different scenarios (e.g. sitting rest, free walking, *etc.*) [54,55]. According to Fig. 4c, h_e also has a great influence on the final results. The MAT is lower when h_e is smaller, and the influence is greater for LET-textile than black cotton. The amount of energy released by the metabolism depends on physical activities. According to ISO EN 8996 [56], the typical q_{gen} values with different activity levels are as follows: for a seated and relaxed person, a seated person with sedentary activity, and a standing person with light activities, the q_{gen} are about 58 W m^{-2}, 70 W m^{-2}, and 116 W m^{-2}, respectively. As shown in Fig. 4d, the higher q_{gen}, the lower MAT. The body motion changes the air gap between skin and textile, which forces the electrons to flow back and forth in LET-textile due to electrostatic induction. Therefore, it is crucial to study how the air gap influences the simulation results. As shown in Fig. 4e, a larger air gap leads to a lower MAT. It is worthwhile to mention that the emissivity of the outer surface of textiles matters more than the inner one because radiation is more dominant in heat transfer between the textile outer surface and the ambient than that between the human body and the textile inner surface [6,11].

Based on the modeling results, when there is no solar radiation, the ambient temperature needs to be 21.0 ℃ to sustain a skin temperature at 33 ℃, while this value is 17.9 ℃ for LET-textile as shown in Fig. 4f. That means the thermostat temperature of buildings in winter could be reduced from 21.0 ℃ to 17.9 ℃ if all the residents wear LET-textiles. EnergyPlus 9.2 was used to model the potential energy savings of a building with such a temperature schedule in which every resident wears LET-textiles. The building model used in this study is a large-size

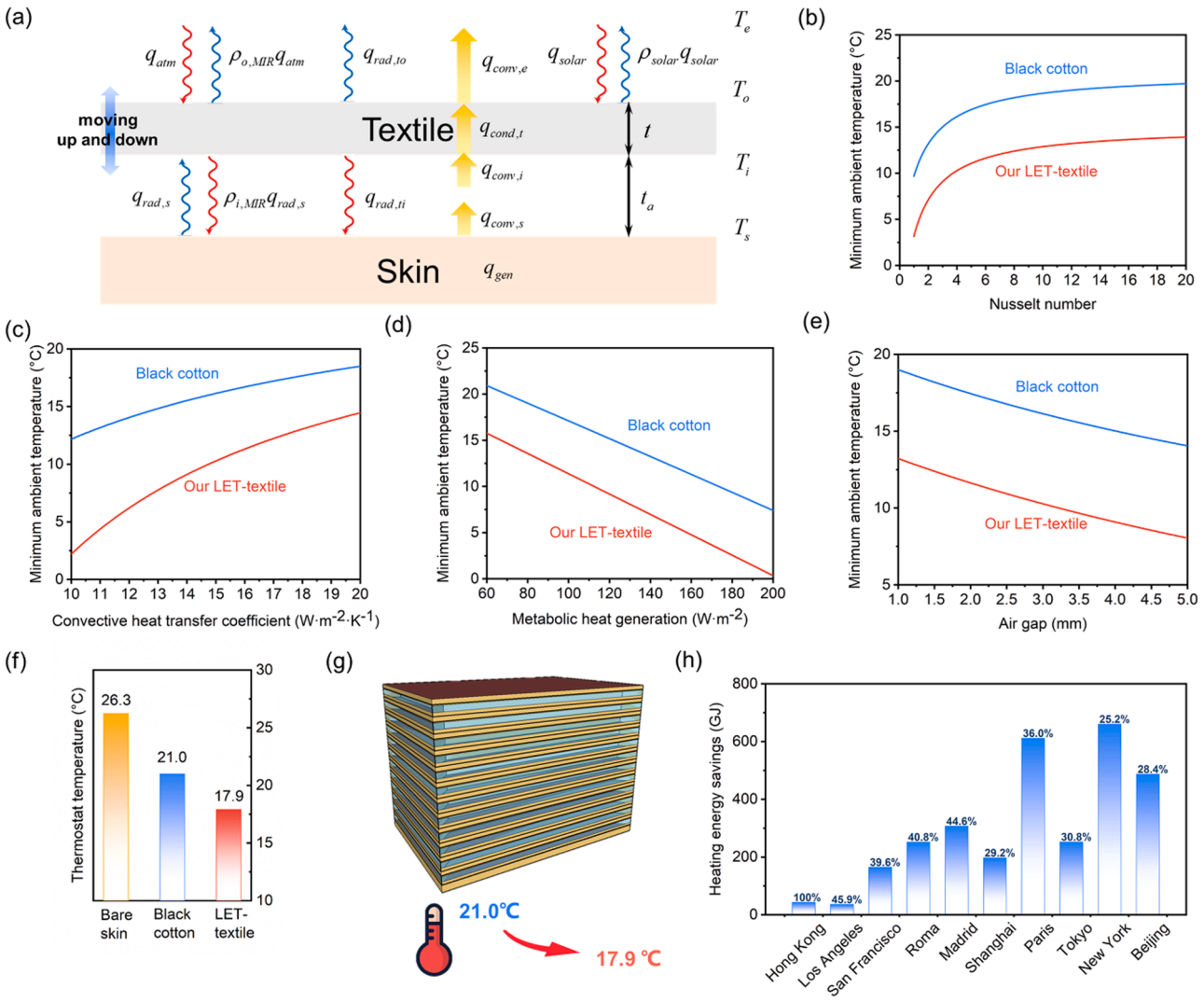

Fig. 4. Heat transfer model and the energy saving potential of LET-textile. (a) Schematic of the heat transfer model. (b) The influence of Nusselt number of the gap between skin and textile on the MAT (q_{gen}=110 W m^{-2}, t_a=3 mm, h_e=15 W m^{-2} K^{-1}, q_{solar}=200 W m^{-2}). (c) The MAT as a function of convective heat transfer coefficient (Nu=4, q_{gen}=110 W m^{-2}, t_a=3 mm, q_{solar}=200 W m^{-2}). (d) The MAT as a function of metabolic heat generation between textile and environment (Nu=4, h_e=15 W m^{-2} K^{-1}, t_a=3 mm, q_{solar}=200 W m^{-2}). (e) The MAT as a function of air gap (Nu=4, q_{gen}=110 W m^{-2}, h_e=15 W m^{-2} K^{-1}, and q_{solar}=200 W m^{-2}). (f) The MAT of bare skin, skin with black cotton, and with the LET-textile. (g) The large-sized office building model. (h) The heating energy saving if the heating setpoint is reduced from 21.0 to 17.9 ℃.

office building (as shown in Fig. 4g) for ten metropolises (Hong Kong, Los Angeles, San Francisco, Roma, Madrid, Shanghai, Paris, Tokyo, New York, and Beijing) across the world, based on the 90.1–2013 benchmark model provided by the U.S. Department of Energy Commercial Reference Buildings Databased [57]. The total heating energy-saving patterns for the selected 10 cities relative to the baseline were determined (Fig. 4h). More heating energy savings were found in cities which have colder winters. 660 GJ, 611 GJ, and 486 GJ of heating energy could be saved in New York, Paris, and Beijing, respectively. As in Hong Kong, the heating energy consumption became zero if LET-textile was used.

2.5. Biomechanical energy harvesting performance of the LET-textile

After demonstrating the passive warming ability of the LET-textile, its biomechanical energy harvesting performance is evaluated as followed. Based on the working mechanism mentioned in Section 2.1, the energy harvesting performances of the LET-textile with an effective dimension of 4.0 × 4.0 cm^2 were investigated systematically. To quantitatively investigate the electric output dependence on various contact frequencies and contact forces between the skin and the textile, a hand was used as the skin [32,58]. When the hand touched the textile, the LET-textile would give positive voltage and current, which means the current move from CT to the ground. While the hand moved away from the textile, it gives negative voltage and current (current move from ground to CT), which is clearly depicted in Fig. 5a and b. The schematic diagrams about how to measure the open-circuit voltage and short-circuit current are shown in Fig. S11 in the supplementary information. The output charges in one cycle were calculated by integrating the current data in Fig. 5b and are shown in Fig. S12 in the supplementary information. The transferred charge for one cycle is about 50 nC. Nanofiber PTFE is important for permeability but not the key factor to affect the output electrical performance, the electrical outputs of the devices using flat surface PTFE and nanofiber PTFE were also compared in Fig. S13 in the supplementary information, and they are almost the same. Fig. 5c and d show the output open-circuit voltage (V_{oc}) and short-circuit current (I_{sc}) by applying a 39 N touching by hand with frequencies of 0.9, 1.1, 1.9, 2.6, and 3.9 Hz. The generated peak voltages correspond to 226, 226, 244, 273, and 286 V. The corresponding peak current are 14.3, 16.9, 18.3, 21.7, and 27.8 μA. The values of V_{oc} and I_{sc} increase as the touch frequency increases, since sufficient charges can

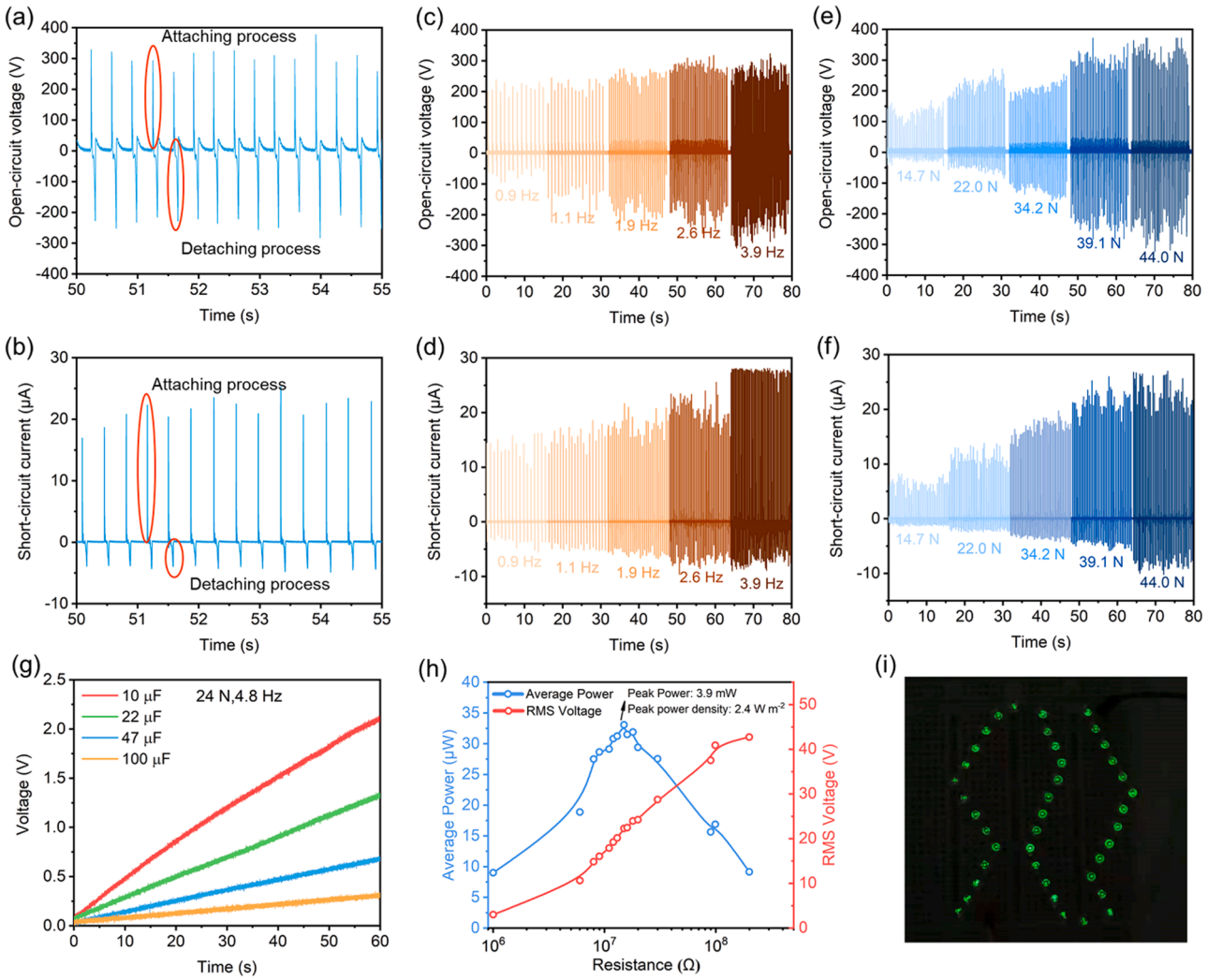

Fig. 5. The bio-mechanical energy harvesting performance of the LET-textile. Typical (a) open-circuit voltages and (b) short-circuit currents generated by the LET-textile. Effect of the loading frequencies (0.9–3.9 Hz) on the electrical output performance of the LET-textile, including (c) open-circuit voltages and (d) short-circuit currents. Effect of the loading forces (14.7–44 N) on the electrical output performance of the LET-textile, including (e) open-circuit voltages and (f) short-circuit currents. (g) Measured voltages of the capacitors (10, 22, 47 and 100 μF) charged by the LET-textile under 24 N and 4.8 Hz tapping. (h) Dependence of voltage and power of the LET-textile on the resistance of an external load under 24 N and 4.8 Hz tapping. (i) Demonstration of lighting up 41 LEDs (the minimum working voltage for each LED is 3 V) by tapping one LET-textile.

only be induced and maintained by enough sequential touch. Fig. 5e and f depict the V_{oc} and I_{sc} of LET-textile under 2.8 Hz with an applied force of 14.7, 22.0, 34.2, 39.1, and 44.0 N, in which peak V_{oc} of 150, 245, 248, 323, and 352 V are achieved, respectively. The corresponding peak I_{sc} attained are 7.5, 12.8, 17.5, 23.4, and 26.2 μA, respectively. The values of V_{oc} and I_{sc} of LET-textile were enhanced by increasing the applied pressing force. Such an enhancement is ascribed to the higher surface friction area between the skin and PTFE under a stronger applied force. Compared with other previously reported textile-TENGs' structures (Table S2 in supporting information), our LET-textile offers a significant improvement in terms of the fabrication process and output performance.

As shown in Fig. 5g, four capacitors with different capacitances were successfully charged by the LET-textile under 24 N and 4.8 Hz. It took 60 s to charge the 10 μF capacitor to 2.1 V. Likewise, 22, 47, and 100 μF capacitors were charged to 1.3, 0.7, and 0.3 V within 60 s, respectively. The output power and output power density of LET-textile were evaluated and calculated as U^2/R and $U^2/(R \bullet A)$ by measuring its output voltage through externally connecting various resistance loads in series under 24 N and 4.8 Hz, where U is the output voltage across the external load, R is the load resistance, and A is the effective contact area. Fig. 5h shows the dependence of output power density on resistances. The root mean square (RMS) voltage increases from 3.0 to 42.7 V as the load resistance increases from 1 to 200 MΩ. The maximum instantaneous power density of 2.4 W m^{-2} was achieved when the load resistance was around 15 MΩ. With such a high performance, LET-textile can light up over 41 LEDs in series by gentle touch as shown in Fig. 5i.

Both robustness and washability are important factors that affect the practical application and lifetime of textile. Hence, stability tests in continuous contact and separation, as well as washability tests were conducted. As shown in Fig. S14 in supporting information, the output current experienced an increase due to the accumulated charges, and then the value became stable after continuously tapping for 20 min (1400 cycles). As shown in Fig. S15, supporting information, the output voltages under the same conditions were unchanged after washing for 3 h by a magnetic bar with a rotational speed of 300 rpm and drying in an oven with 60 °C. This remarkable durability of LET-textile makes it promising for real-world applications.

3. Conclusions

In summary, we demonstrated a versatile nanophotonic TENG

textile. The textile uses TiN NPs to harvest solar radiation for body warming and PTFE nanofiber membrane as the tribo-negative friction material for electricity generation. Conductive textile is significantly important in this design since it not only served as a low-emissivity substrate to suppress radiative heat dissipation for passive radiative warming but also as an electrode for TENG. Since the simple fabrication methods, the textile can be readily produced in a large area. This textile design achieves a low thermal emissivity down to 11.0% and high solar absorptivity up to 83.7%. The textile could be worn at a low ambient temperature of 5 ℃ with a weak solar irradiance of 400 W m^{-2} while keeping the body temperature above 33 ℃. Such a textile enables a 3 ℃ decrease in the indoor setpoint compared to traditional cotton textile. Such a 3 ℃ setpoint reduction can potentially result in building heating energy savings of 25.2–100%, according to EnergyPlus simulations. In addition, our textile can harvest biomechanical energy and get 150 V and 7.5 μA under 15 N and 2.8 Hz tapping. A peak power density of 2.4 W m^{-2} was achieved under 24 N and 4.8 Hz tapping. This energy could be used to power LEDs or restored in capacitors and then to power wearable electronics. We believe that this radiative warming TENG textile with supreme performance can provide power to wearable electronics and at the same time guarantee thermal comfort. Future work will be conducted to develop a textile that can dynamically change the emissivity of the textile to overcome the overheating problem by using an electrochromic textile powered by textile-TENG.

4. Experimental section

4.1. Fabrication of LET-textile

First of all, the colloidal TiN solution was prepared referring to the previous work [41]. Commercial TiN NPs with a size of 20 nm (Aladdin Bio-Chem Technology, Shanghai) were added to the propylene glycol methyl ether acetate (PGMEA, $C_6H_{12}O_3$, Aladdin Bio-Chem Technology, Shanghai). Their mixture with 20 wt% TiN NPs was treated by ultrasonic dispersion technique for 1 h and then treated by high-energy ball milling for at least 10 h. The obtained well-dispersed colloid was diluted to 1 wt% by adding ethanol solvent.

Before the spray-coating process, the Cu/Ni conductive textile was treated by plasma to improve its wettability. After that, TiN NPs solutions were spray-coated on the textile using a precise ultrasonic spray coating machine (UC330, Siansonic Technology, China). The frequency of the ultrasonic nozzle was 45 kHz, and the power was 1.5 W. The flow rate of the solution was 0.1 or 0.2 ml min^{-1}. The spray nozzle was held at 80 mm above the surface and the spray width was 6 mm. The moving speed of the spray nozzle was set as 120 mm/s in the X-Y plane to achieve homogeneous deposition of the TiN nanoparticles. The substrate temperature was set as 60 °C to accelerate solvent evaporation. For each sample, the spraying process was repeated a lot of runs, specifically, 12, 30, 50, 60, 90, and 120 runs at a flow rate of 0.1 ml min^{-1}, as well as 20, 30, 40, and 50 runs at a flow rate of 0.2 ml min^{-1}. Finally, the nanofiber PTFE membrane (PTFE23001, Sterlitech, USA) was attached to the other side of the conductive textile by hot pressing with a thin non-woven glue film as the adhesive layer.

4.2. Characterization

The surface morphologies of the textiles were observed using a scanning electron microscope (JSM-7100F, Jeol). The UV/visible/near-IR (0.3–2.5 μm) reflectivity (R) and transmittance (T) spectra of the textiles were measured using a spectrometer (Lambda 950, Perkin Elmer) equipped with a 150 mm integrating sphere. The mid-IR reflectance and transmittance spectra were measured using a Fourier transform infrared spectrometer (Vertex 70, Bruker) with a golden integrating sphere. The absorptivity/emissivity spectra (A) were directly derived from $1\text{-}R\text{-}T$. The sheet resistance of the conductive fabric was investigated using the four-probe method. The IR thermal image was taken by an IR camera (Ti480 Pro, Fluke). The tensile, tearing, and cyclic tensile test was measured by a tensile tester (Zwick Roell, German). All the measurements were conducted in an environment with constant temperature (24 ℃) and humidity (50%). For the tensile test, the LET-textile sample was cut into a dumbbell-shaped sample (as shown in Fig. S10a in the supplementary information) with a gauge length of 25.6 mm and a width of 4.5 mm. The displacement rate was 100%/min. Tearing tests were performed to quantify the fracture energy of the LET-textile. Samples (16 mm width × 90 mm length) were cut into a trouser shape with an initial notch length of about 40 mm. The two arms of the sample were mounted on the clamps. The upper clamp was loaded at a constant low velocity of 1.7 mm/s, and the corresponding tearing force F was recorded. The fracture energy Γ was calculated by $\Gamma = 2F/\omega$, where ω is the thickness of the sample and F is the average tearing force when cracks propagate. Cyclic tensile tests were performed to test the shape recovery property of LET-textile. The dumbbell-shaped sample was loaded-unloaded 3 consecutive times up to 15% strain, and the stress and strain were measured. An index to quantitatively measure the shape recovery from the cyclic tensile test is defined as r, and equals to $\frac{\varepsilon_x-\varepsilon_y}{\varepsilon_x-\varepsilon_z}\times 100\%$, where ε_x, ε_y, and ε_z represent the maximum strain in the cycle, the residual strain after unloading, and the strain before loading, respectively.

4.3. Air permeability test

The testing procedure is based on ASTM D737 with modification. Textiles samples were put inside a wind tunnel with a rectangular cross-section. The exposed area of textile is 2 cm × 4 cm. There are two openings on the wind tunnel before and after the textile. A differential pressure gauge (Velocicalc multifunction meter model 9565, TSI, USA) was connected to both openings to measure the pressure drops across the textile sample at different air flow rates. The schematic diagram of the setup is shown in Fig. S1a in supporting information.

4.4. Water vapor transmission rate test

The testing procedure is based on ASTM E96 with modification. Glass bottles (100 ml) were filled with 60 ml distilled water. The bottles were sealed by the textile samples using open-top caps, and silicone gaskets (Corning). The exposed area of the textile is 3 cm in diameter. The sealed bottles were then placed into an environmental chamber, in which the temperature was held at 35 ℃ and the relative humidity was 30%. The mass of the bottles was measured periodically, and the reduced mass should come from the evaporated water. The reduced mass was then divided by the area to derive the water vapor transmission.

4.5. Energy generation measurement

In order to measure the output electric performance of LET-textile under different touching situations with skin, the hands tapping motion with different forces (14.7–44.0 N) and frequencies (1.0–4.0 Hz) were applied. The forces were measured by a force sensing resistor (FSR01, OHMITE, USA). The output current was measured by an electrometer (Keithley 6514), and the output voltage was analyzed by a digital oscilloscope (Tektronix TDS 2024 C) with a high voltage probe (Tektronix P5100A) with 40 $M\Omega$ input impedance.

4.6. Warming performance measurement

Warming performance tests were conducted in an environmental control room (DBT and WBT ± 0.1 °C) in Hong Kong University of Science and Technology (HKUST). A black cotton with a thickness of 600 μm was also tested for comparison. Several layers of CT textiles were pressed together to obtain the same thickness (600 μm) with the cotton. The solar warming performance was evaluated under the

illumination of a solar simulator (Oriel Sol2A, Newport) using a xenon lamp. For the warming performance tests, the solar simulator was shut down. The input power was ~ 110 W m^{-2} by a source meter. This is determined by keeping the bare skin at 33 °C at the ambient temperature of 25 °C. The input current and voltage were calibrated by a high-precision multimeter (FLUKE 289). T-type thermal couples, which were connected to a data acquisition device (NI9213, National Instrument), were attached on the backside of samples to measure the steady-state temperatures. The temperature data were recorded every two seconds.

4.7. Energy consumption simulation

The energy-saving potential of the LET-textile is estimated using EnergyPlus 9.2 in reference to a large-sized office building. With 10 stories, each floor of the building is divided into five zones: a core zone surrounded by four exterior rooms at four orientations. An occupant density of 18.58 m^2 per person, with occupancy primarily between the hours of 08:00 and 17:00 on weekdays, is defined. The lighting and electrical equipment loads are 8.83 W m^{-2} and 8.07 W m^{-2}, respectively. The office building utilizes individual variable air volume (VAV) systems to condition each floor. Each VAV loop consists of a cooling coil and a heating coil fed by a centralized water-cooled centrifugal chiller, and a gas boiler respectively. Reheat air terminals in each zone provide humidity control for occupancy comfort.

CRediT authorship contribution statement

Yi Zhang: Conceptualization, Methodology, Writing – original draft. **Yang Li**: Conceptualization, Methodology, Writing – original draft. **Keqiao Li**: Validation, Investigation. **Ye Seul Kwon**: Validation, Investigation. **Thilhara Tennakoon**: Validation. **Cunteng Wang**: Validation. **Ka Chung Chan**: Resources, Writing – review & editing. **Sau-Chung Fu**: Resources, Writing – review & editing. **Baoling Huang**: Supervision, Project administration. **Christopher Y.H. Chao**: Supervision, Project administration, Funding acquisition.

Declaration of Competing Interest

The authors declare that they have no known competing financial interests or personal relationships that could have appeared to influence the work reported in this paper.

Acknowledgments

The work was supported by the General Research Fund (GRF) (project No. 17205419) granted by the Research Grants Council of the Hong Kong Special Administrative Region, China.

Appendix A. Supplementary material

Supplementary data associated with this article can be found in the online version at doi:10.1016/j.nanoen.2022.106996.

References

[1] L.F. Cabeza, A. de Gracia, 20 – Thermal energy storage systems for cooling in residential buildings, in: L.F. Cabeza (Ed.), Advances in Thermal Energy Storage Systems, second ed., Woodhead Publishing, 2021, pp. 595–623.
[2] D. Ürge-Vorsatz, N. Eyre, P. Graham, D. Harvey, E. Hertwich, Y. Jiang, C. Kornevall, M. Majumdar, J.E. McMahon, S. Mirasgedis, Energy End-Use: Buildings, Global Energy Assessment: Toward a Sustainable Future, Cambridge University Press, 2012, pp. 649–760.
[3] H. Luo, Q. Li, K. Du, Z. Xu, H. Zhu, D. Liu, L. Cai, P. Ghosh, M. Qiu, An ultra-thin colored textile with simultaneous solar and passive heating abilities, Nano Energy 65 (2019), 103998.
[4] P.C. Hsu, C. Liu, A.Y. Song, Z. Zhang, Y. Peng, J. Xie, K. Liu, C.L. Wu, P.B. Catrysse, L. Cai, S. Zhai, A. Majumdar, S. Fan, Y. Cui, A dual-mode textile for human body radiative heating and cooling, Sci. Adv. 3 (2017), e1700895.
[5] Y. Peng, Y. Cui, Advanced textiles for personal thermal management and energy, Joule 4 (2020) 724–742.
[6] L. Cai, A.Y. Song, P. Wu, P.C. Hsu, Y. Peng, J. Chen, C. Liu, P.B. Catrysse, Y. Liu, A. Yang, C. Zhou, C. Zhou, S. Fan, Y. Cui, Warming up human body by nanoporous metallized polyethylene textile, Nat. Commun. 8 (2017) 496.
[7] H. Luo, Y. Zhu, Z. Xu, Y. Hong, P. Ghosh, S. Kaur, M. Wu, C. Yang, M. Qiu, Q. Li, Outdoor personal thermal management with simultaneous electricity generation, Nano Lett. 21 (2021) 3879–3886.
[8] W. Wang, H. Wen, X. Huan, J. Su, W. Wang, J. Shi, C. Wang, One-step reactive sputtering of novel MoOx nanogradient absorber for flexible and wearable personal passive heating, Sol. RRL 4 (2020), 2000055.
[9] M. Shi, M. Shen, X. Guo, X. Jin, Y. Cao, Y. Yang, W. Wang, J. Wang, Ti3C2Tx MXene-decorated nanoporous polyethylene textile for passive and active personal precision heating, ACS Nano 15 (2021) 11396.
[10] P.C. Hsu, A.Y. Song, P.B. Catrysse, C. Liu, Y. Peng, J. Xie, S. Fan, Y. Cui, Radiative human body cooling by nanoporous polyethylene textile, Science 353 (2016) 1019.
[11] X. Li, W. Xie, C. Sui, P.C. Hsu, Multispectral thermal management designs for net-zero energy buildings, ACS Mater. Lett. 2 (2020) 1624–1643.
[12] J.D. Hardy, E.F. DuBois, Regulation of heat loss from the human body, Proc. Natl. Acad. Sci. USA 23 (1937) 624.
[13] C.E. Winslow, A. Gagge, L. Herrington, The influence of air movement upon heat losses from the clothed human body, Am. J. Physiol. Leg. Content 127 (1939) 505–518.
[14] X.A. Zhang, S. Yu, B. Xu, M. Li, Z. Peng, Y. Wang, S. Deng, X. Wu, Z. Wu, M. Ouyang, Y. Wang, Dynamic gating of infrared radiation in a textile, Science 363 (2019) 619.
[15] Y. Guo, X. Zhang, Y. Wang, W. Gong, Q. Zhang, H. Wang, J. Brugger, All-fiber hybrid piezoelectric-enhanced triboelectric nanogenerator for wearable gesture monitoring, Nano Energy 48 (2018) 152–160.
[16] J. Wang, S. Li, F. Yi, Y. Zi, J. Lin, X. Wang, Y. Xu, Z.L. Wang, Sustainably powering wearable electronics solely by biomechanical energy, Nat. Commun. 7 (2016) 12744.
[17] C. Shi, Z. Zou, Z. Lei, P. Zhu, W. Zhang, J. Xiao, Heterogeneous integration of rigid, soft, and liquid materials for self-healable, recyclable, and reconfigurable wearable electronics, Sci. Adv. 6 (2020) eabd0202.
[18] Y. Lee, J. Park, A. Choe, S. Cho, J. Kim, H. Ko, Mimicking human and biological skins for multifunctional skin electronics, Adv. Funct. Mater. 30 (2020), 1904523.
[19] X. Pu, L. Li, H. Song, C. Du, Z. Zhao, C. Jiang, G. Cao, W. Hu, Z.L. Wang, A. Self-Charging, Power unit by integration of a textile triboelectric nanogenerator and a flexible lithium-ion battery for wearable electronics, Adv. Mater. 27 (2015) 2472–2478.
[20] Y. Niu, H. Liu, R. He, Z. Li, H. Ren, B. Gao, H. Guo, G.M. Genin, F. Xu, The new generation of soft and wearable electronics for health monitoring in varying environment: from normal to extreme conditions, Mater. Today 41 (2020) 219–242.
[21] J.H. Koo, S. Jeong, H.J. Shim, D. Son, J. Kim, D.C. Kim, S. Choi, J.-I. Hong, D.-H. Kim, Wearable electrocardiogram monitor using carbon nanotube electronics and color-tunable organic light-emitting diodes, ACS Nano 11 (2017) 10032–10041.
[22] Y. Liu, M. Pharr, G.A. Salvatore, Lab-on-skin: a review of flexible and stretchable electronics for wearable health monitoring, ACS Nano 11 (2017) 9614–9635.
[23] H. Wang, Y. Zhang, X. Liang, Y. Zhang, Smart fibers and textiles for personal health management, ACS Nano 15 (2021) 12497–12508.
[24] Z. Wen, M. Yeh, H. Guo, J. Wang, Y. Zi, W. Xu, J. Deng, L. Zhu, X. Wang, C. Hu, L. Zhu, X. Sun, Z.L. Wang, Self-powered textile for wearable electronics by hybridizing fiber-shaped nanogenerators, solar cells, and supercapacitors, Sci. Adv. 2 (2016), e1600097.
[25] K. Dong, X. Peng, Z.L. Wang, Fiber/fabric-based piezoelectric and triboelectric nanogenerators for flexible/stretchable and wearable electronics and artificial intelligence, Adv. Mater. 32 (2020), 1902549.
[26] G. Chen, Y. Li, M. Bick, J. Chen, Smart textiles for electricity generation, Chem. Rev. 120 (2020) 3668–3720.
[27] Y. Liu, L. Yin, W. Zhang, J. Wang, S. Hou, Z. Wu, Z. Zhang, C. Chen, X. Li, H. Ji, Q. Zhang, Z. Liu, F. Cao, A wearable real-time power supply with a Mg3Bi2-based thermoelectric module, Cell Rep. Phys. Sci. 2 (2021), 100412.
[28] M. Zhu, M. Lou, J. Yu, Z. Li, B. Ding, Energy autonomous hybrid electronic skin with multi-modal sensing capabilities, Nano Energy 78 (2020), 105208.
[29] M. Zhu, Y. Wang, M. Lou, J. Yu, Z. Li, B. Ding, Bioinspired transparent and antibacterial electronic skin for sensitive tactile sensing, Nano Energy 81 (2021), 105669.
[30] Y. Wang, M. Zhu, X. Wei, J. Yu, Z. Li, B. Ding, A dual-mode electronic skin textile for pressure and temperature sensing, Chem. Eng. J. 425 (2021), 130599.
[31] Z. Yan, L. Wang, Y. Xia, R. Qiu, W. Liu, M. Wu, Y. Zhu, S. Zhu, C. Jia, M. Zhu, R. Cao, Z. Li, X. Wang, Flexible high-resolution triboelectric sensor array based on patterned laser-induced graphene for self-powered real-time tactile sensing, Adv. Funct. Mater. 31 (2021), 2100709.
[32] J. Xiong, P. Cui, X. Chen, J. Wang, K. Parida, M.F. Lin, P.S. Lee, Skin-touch-actuated textile-based triboelectric nanogenerator with black phosphorus for durable biomechanical energy harvesting, Nat. Commun. 9 (2018) 4280.
[33] W. Seung, M.K. Gupta, K.Y. Lee, K.-S. Shin, J.H. Lee, T.Y. Kim, S. Kim, J. Lin, J. H. Kim, S.W. Kim, Nanopatterned textile-based wearable triboelectric nanogenerator, ACS Nano 9 (2015) 3501–3509.
[34] S. Lee, W. Ko, Y. Oh, J. Lee, G. Baek, Y. Lee, J. Sohn, S. Cha, J. Kim, J. Park, J. Hong, Triboelectric energy harvester based on wearable textile platforms employing various surface morphologies, Nano Energy 12 (2015) 410–418.

[35] J. Yi, K. Dong, S. Shen, Y. Jiang, X. Peng, C. Ye, Z.L. Wang, Fully fabric-based triboelectric nanogenerators as self-powered human–machine interactive keyboards, Nano-Micro Lett. 13 (2021) 103.
[36] S.S. Kwak, H.J. Yoon, S.W. Kim, Textile-based triboelectric nanogenerators for self-powered wearable electronics, Adv. Funct. Mater. 29 (2019), 1804533.
[37] R. Cheng, K. Dong, L. Liu, C. Ning, P. Chen, X. Peng, D. Liu, Z.L. Wang, Flame-retardant textile-based triboelectric nanogenerators for fire protection applications, ACS Nano 14 (2020) 15853–15863.
[38] M. Zhu, Q. Shi, T. He, Z. Yi, Y. Ma, B. Yang, T. Chen, C. Lee, Self-powered and self-functional cotton sock using piezoelectric and triboelectric hybrid mechanism for healthcare and sports monitoring, ACS Nano 13 (2019) 1940–1952.
[39] Y. Song, N. Wang, C. Hu, Z.L. Wang, Y. Yang, Soft triboelectric nanogenerators for mechanical energy scavenging and self-powered sensors, Nano Energy 84 (2021), 105919.
[40] H. Zou, Y. Zhang, L. Guo, P. Wang, X. He, G. Dai, H. Zheng, C. Chen, A.C. Wang, C. Xu, Z.L. Wang, Quantifying the triboelectric series, Nat. Commun. 10 (2019) 1427.
[41] Y. Li, C. Lin, Z. Wu, Z. Chen, C. Chi, F. Cao, D. Mei, H. Yan, C.Y. Tso, C.Y.H. Chao, B. Huang, Solution-processed all-ceramic plasmonic metamaterials for efficient solar–thermal conversion over 100–727 °C, Adv. Mater. 33 (2021), 2005074.
[42] W. Yang, W. Gong, C. Hou, Y. Su, Y. Guo, W. Zhang, Y. Li, Q. Zhang, H. Wang, All-fiber tribo-ferroelectric synergistic electronics with high thermal-moisture stability and comfortability, Nat. Commun. 10 (2019) 1–10.
[43] X. Peng, K. Dong, C. Ye, Y. Jiang, S. Zhai, R. Cheng, D. Liu, X. Gao, J. Wang, Z. L. Wang, A breathable, biodegradable, antibacterial, and self-powered electronic skin based on all-nanofiber triboelectric nanogenerators, Sci. Adv. 6 (2020) eaba9624.
[44] X. Guan, B. Xu, M. Wu, T. Jing, Y. Yang, Y. Gao, Breathable, washable and wearable woven-structured triboelectric nanogenerators utilizing electrospun nanofibers for biomechanical energy harvesting and self-powered sensing, Nano Energy 80 (2021), 105549.
[45] M. Sala de Medeiros, D. Chanci, C. Moreno, D. Goswami, R.V. Martinez, Waterproof, breathable, and antibacterial self-powered e-textiles based on omniphobic triboelectric nanogenerators, Adv. Funct. Mater. 29 (2019), 1904350.
[46] W. Gong, X. Wang, W. Yang, J. Zhou, X. Han, M.D. Dickey, Y. Su, C. Hou, Y. Li, Q. Zhang, Wicking–polarization-induced water cluster size effect on triboelectric evaporation textiles, Adv. Mater. 33 (2021), 2007352.
[47] D.W. Kim, J.H. Lee, J.K. Kim, U. Jeong, Material aspects of triboelectric energy generation and sensors, NPG Asia Mater. 12 (2020) 6.
[48] B. Meng, X. Cheng, X. Zhang, M. Han, W. Liu, H. Zhang, Single-friction-surface triboelectric generator with human body conduit, Appl. Phys. Lett. 104 (2014), 103904.
[49] B. Meng, W. Tang, Z. Too, X. Zhang, M. Han, W. Liu, H. Zhang, A transparent single-friction-surface triboelectric generator and self-powered touch sensor, Energy Environ. Sci. 6 (2013) 3235–3240.
[50] G.V. Naik, J.L. Schroeder, X. Ni, A.V. Kildishev, T.D. Sands, A. Boltasseva, Titanium nitride as a plasmonic material for visible and near-infrared wavelengths, Opt. Mater. Express 2 (2012) 478–489.
[51] Y. Li, C. Xiong, H. Huang, X. Peng, D. Mei, M. Li, G. Liu, M. Wu, T. Zhao, B. Huang, 2D Ti3C2Tx MXenes: visible black but infrared white materials, Adv. Mater. 33 (2021), 2103054.
[52] J.K. Tong, X. Huang, S.V. Boriskina, J. Loomis, Y. Xu, G. Chen, Infrared-transparent visible-opaque fabrics for wearable personal thermal management, ACS Photonics 2 (2015) 769–778.
[53] F. Wang, Clothing Evaporative Resistance: Its Measurements and Application in Prediction of Heat Strain, Lund University, 2011.
[54] A. Gaspar, A. Oliveira, D. Quintela, Effects of walking and air velocity on convective heat transfer from a nude manikin, in: Proceedings of the Winsdor Conference: Comfort and Energy Use in Buildings: Getting Them Right–International Conference, Windsor Great Park, UK, 2006, pp. 27–30.
[55] A.P. Gagge, R.R. Gonzalez, Mechanisms of heat exchange: biophysics and physiology, in: R. Terjung (Ed.) Comprehensive Physiology, 2011, pp. 45–84.
[56] R. Hu, Y. Liu, S. Shin, S. Huang, X. Ren, W. Shu, J. Cheng, G. Tao, W. Xu, R. Chen, Emerging materials and strategies for personal thermal management, Adv. Energy Mater. 10 (2020), 1903921.
[57] M. Deru, K. Field, D. Studer, K. Benne, B. Griffith, P. Torcellini, B. Liu, M. Halverson, D. Winiarski, M. Rosenberg, US Department of Energy Commercial Reference Building Models of the National Building Stock, National Renewable Energy Laboratory, Golden, CO, 2011.
[58] Y. Wu, Y. Luo, J. Qu, W.A. Daoud, T. Qi, Liquid single-electrode triboelectric nanogenerator based on graphene oxide dispersion for wearable electronics, Nano Energy 64 (2019), 103948.

Yi Zhang received his B.S. degree from Xi'an Jiaotong University in 2017 and MPhil degree from The Hong Kong University of Science and Technology in 2019. He is currently a Ph. D. candidate at the Department of Mechanical Engineering at the University of Hong Kong. His research interests include smart textile, triboelectric nanogenerator, and green building techniques.

Yang Li received his B.S. degree from Huazhong University of Science and Technology in 2012 and M.S. degree from Zhejiang University in 2015. After that, He received his Ph.D. degree in the Department of Mechanical and Aerospace Engineering from The Hong Kong University of Science and Technology (HKUST) in 2019. He is currently a postdoctoral research fellow in HKUST. His research interests include solar-thermal energy conversion, spectrally selective metasurfaces, and plasmonic metamaterials.

Keqiao Li received his B.S. and M.S. degree from Huazhong University of Science and Technology in 2015 and 2018. He is currently a Ph.D. candidate at the Department of Mechanical and Aerospace Engineering in the Hong Kong University of Science and Technology (HKUST). His research interests include smart textiles for personal thermal management and spectrally selective metasurfaces.

Ye Seul Kwon received her B.S. degree in Mechanical Engineering from The Hong Kong University of Science and Technology in 2020. She is currently a M.Phil. student in Prof. Baoling Huang's group. Her current research is mainly on the scalable solar absorber and its practical applications.

Thilhara Tennakoon received her BEng ME degree from the University of Hong Kong (HKU) in 2019. She works as a Research Assistant in the Advanced Thermodynamics and Environmental Engineering laboratory at HKU. Her research interests include engineering sustainability and acoustofluidics.

Cunteng Wang received his B.S. degree from Zhengzhou University in 2014, Master degree from Harbin Institute of Technology in 2017, and Ph.D. degree from The Hong Kong University of Science and Technology in 2020. He is currently a Research Associate at The University of Hong Kong. His research interests include aerosol and fluid dynamics.

Dr. Ka Chung Chan is a Postdoctoral Scholar at The University of Hong Kong. He received his Bachelor's, MPhil and Ph.D. degree in Mechanical Engineering from The Hong Kong University of Science and Technology in 2009, 2011 and 2015, respectively. His research area includes energy and thermal systems, adsorption technology, energy sustainability and thermal fluidic simulation.

Dr. Sau-Chung Fu is a research assistant professor in the Department of Mechanical Engineering, HKU. He received his BEng and MPhil in Mechanical Engineering from the University of Hong Kong in 1999 and 2001 respectively. After practiced for some years in an engineering consultant, he went on pursuing a Ph.D. degree in Mechanical Engineering at the Hong Kong Polytechnic University in 2011. Dr. Fu's research focused on aerosol and bioaerosol, nanofluids and heat exchanger, turbulent flow, computational fluid dynamics, wind power systems, and ventilation systems.

Baoling Huang is currently an Associate Professor in The Hong Kong University of Science and Technology. He received his B. S. and M.S. degrees from Tsinghua University, China in 1999 and 2001. He worked in industry from 2001 to 2004. In 2008, he received his Ph.D. degree in Mechanical Engineering from the University of Michigan, Ann Arbor, USA. Then, he worked as a postdoctoral research fellow at the University of California, Berkeley and Lawrence Berkeley National Laboratory. His research interests are in the broad area of energy transport, conversion and storage.

Prof. Christopher Y.H. Chao is Vice President (Research and Innovation) and Chair Professor of Thermal and Environmental Engineering of The Hong Kong Polytechnic University. He received his BSc(Eng) degree in Mechanical Engineering (First Class) from HKU in 1988. He obtained his M.S. and Ph.D. degrees in Mechanical Engineering from The University of California, Berkeley, USA, in 1992 and 1994, respectively. He has a wide range of research interests in the areas of built environment, energy and environmental engineering. He is a fellow of a number of professional societies (FASME, FIMechE, FCIBSE, FISIAQ, FHKEng, FHKIE).